PORTLAND PRESS

Research Article

Cycloserine enantiomers are reversible inhibitors of human alanine:glyoxylate aminotransferase: implications for primary hyperoxaluria type 1

Mirco Dindo[1,2,*], Silvia Grottelli[1,*], Giannamaria Annunziato[3], Giorgio Giardina[4], Marco Pieroni[3], Gioena Pampalone[1], Andrea Faccini[5], Francesca Cutruzzolà[4], Paola Laurino[2], Gabriele Costantino[3,5] and Barbara Cellini[1]

[1]Department of Experimental Medicine, University of Perugia, Perugia, Italy; [2]Okinawa Institute of Science and Technology Graduate University, 1919-1 Tancha, Onna-son, Okinawa 904-0412, Japan; [3]P4T Group, Department of Food and Drug, University of Parma, Parma, Italy; [4]Department of Biochemical Sciences 'A. Rossi Fanelli', Sapienza University of Rome, Rome, Italy; [5]Centro Interdipartimentale Misure G. Casnati, Parco Area Delle Scienze 23, University of Parma, Parma, Italy

Correspondence: Barbara Cellini (barbara.cellini@unipg.it) or Mirco Dindo (mirco.dindo@unipg.it)

Peroxisomal alanine:glyoxylate aminotransferase (AGT) is responsible for glyoxylate detoxification in human liver and utilizes pyridoxal 5′-phosphate (PLP) as coenzyme. The deficit of AGT leads to Primary Hyperoxaluria Type I (PH1), a rare disease characterized by calcium oxalate stones deposition in the urinary tract as a consequence of glyoxylate accumulation. Most missense mutations cause AGT misfolding, as in the case of the G41R, which induces aggregation and proteolytic degradation. We have investigated the interaction of wild-type AGT and the pathogenic G41R variant with ᴅ-cycloserine (DCS, commercialized as Seromycin), a natural product used as a second-line treatment of multidrug-resistant tuberculosis, and its synthetic enantiomer ʟ-cycloserine (LCS). In contrast with evidences previously reported on other PLP-enzymes, both ligands are AGT reversible inhibitors showing inhibition constants in the micromolar range. While LCS undergoes half-transamination generating a ketimine intermediate and behaves as a classical competitive inhibitor, DCS displays a time-dependent binding mainly generating an oxime intermediate. Using a mammalian cellular model, we found that DCS, but not LCS, is able to promote the correct folding of the G41R variant, as revealed by its increased specific activity and expression as a soluble protein. This effect also translates into an increased glyoxylate detoxification ability of cells expressing the variant upon treatment with DCS. Overall, our findings establish that DCS could play a role as pharmacological chaperone, thus suggesting a new line of intervention against PH1 based on a drug repositioning approach. To a widest extent, this strategy could be applied to other disease-causing mutations leading to AGT misfolding.

Introduction

Alanine:glyoxylate aminotransferase (AGT, EC 2.6.1.44) catalyzes the conversion of ʟ-alanine and glyoxylate into pyruvate and glycine in liver peroxisomes, using pyridoxal 5′-phosphate (PLP) as coenzyme [1]. The deficit of AGT, as a consequence of inherited mutations on the *AGXT* gene, leads to accumulation of glyoxylate that is eventually oxidized to oxalate, a metabolic end-product that precipitates as calcium oxalate (CaOx) stones in the kidneys and, in the most severe forms, in the whole body. This rare condition is named Primary Hyperoxaluria Type I (PH1, OMIM 259900) [2,3]. PH1 patients are currently treated by liver transplantation, a procedure coming with serious side effects, or by the administration of pyridoxine, a precursor of PLP effective in a minority (30%) of patients [4–6].

AGT is homodimeric and belongs to the Fold Type I family of PLP-dependent enzymes. The two subunits interact through an extensive core interface, as well as through an N-terminal extension wrapped over the neighboring monomer. The active site is made up of residues coming from both subunits and PLP is covalently bound through a Schiff base linkage with Lys209 [7]. The AGT catalytic mechanism is typical of PLP-dependent aminotransferases and comprises two half-reactions [1]. In the first one, the α-amino group of the substrate L-alanine displaces the ε-amino group of Lys209 producing the external aldimine. Then, Lys209 acts as a general base for the 1,3-prototropic shift generating a ketimine intermediate, which hydrolyzes to pyruvate and pyridoxamine 5′-phosphate (PMP) [8]. In the second half-reaction, glyoxylate binds to AGT–PMP and, through the same steps of the first reaction but in a reverse order, is converted to glycine regenerating AGT–PLP.

PH1 is an extremely heterogenous disease from a genetic point of view (∼200 pathogenic mutations are known) [9]. Nevertheless, biochemical and cell biology studies agree upon the view that most missense mutations cause folding defects in AGT that can result in (i) an increased aggregation propensity, either in the cytosol or inside peroxisomes, (ii) a reduced stability of the dimeric structure, (iii) an increased susceptibility to proteolytic degradation, and/or (iv) a mislocalization of the protein to mitochondria for mutations co-inherited with the polymorphic P11L mutation that generates a putative mitochondrial targeting sequence. For these reasons, PH1 is referred as a misfolding disease [10,11].

The use of small molecules that bind a target protein and enable its proper folding, namely pharmacological chaperones (PCs), is a promising strategy to treat misfolding diseases. PCs have been successfully applied to treat lysosomal storage disorders, phenylketonuria, tyrosine hydroxylase deficiency, cystic fibrosis, nephrogenic diabetes insipidus [12]. In the case of enzymatic deficits, they are usually competitive inhibitors of the target enzyme. This approach has been also explored in PH1. Aminooxyacetic acid is a well-known AGT inhibitor behaving as chaperone to rescue some of the most common mutations leading to PH1, but its low specificity makes it unsuitable for *in vivo* applications [13]. To identify potential PCs specific for AGT, we looked for known inhibitors of PLP-enzymes approved for clinical use. Among them, cycloserine (CS) is a cyclic analog of alanine or serine able to bind many PLP-dependent enzymes including transaminases, racemases and decarboxylases [14–19]. The two enantiomers of CS (Figure 1) show different properties. D-cycloserine (DCS) is a broad-spectrum antibiotic isolated from *Streptomyces sp.* strains used as a second-line drug in combination therapies to treat tuberculosis, whose main target is alanine racemase [15,18]. DCS is also used in neurological studies for its ability to behave as an agonist of NMDA receptors [20]. L-cycloserine (LCS) is the synthetic enantiomer of CS commonly used as a regulator of lipid metabolism in cellular studies [21]. A common feature of LCS and DCS is that they are considered irreversible inhibitors of PLP-enzymes, because they form stable covalent adducts with the cofactor. In some cases, like in branched-chain aminotransferase, alanine racemase, and serine palmitoyl transferase [14,15,17], both LCS and DCS behave as inhibitors, although with different kinetic properties.

Using a combination of UV-Vis spectroscopy, enzyme kinetics, x-ray crystallography, and mass spectrometry, here we explored the interaction of the two CS enantiomers with wild-type AGT and the G41R pathogenic variant showing a folding defect leading to an increased tendency to aggregation and degradation [22,23]. Surprisingly, we found that both LCS and DSC behave as reversible competitive inhibitors, although the stereochemistry of the ligand influences inhibition kinetics and mechanism. Studies in a cellular model demonstrate that DCS, but not LCS, behaves as PC for the G41R variant. The significance of the results obtained for the general mechanism of inhibition of PLP-enzymes by CS, as well as for the possible future use of the CS chemical scaffold for the development of more specific PCs is discussed.

Materials and methods
Materials
PLP, L-alanine, sodium glyoxylate, rabbit muscle L-lactic dehydrogenase (LDH), β-Nicotinamide adenine dinucleotide (NADH), isopropyl-β-D-thiogalactoside (IPTG), LCS, DCS and imidazole were all purchased from Sigma. Ham's F12 Glutamax medium and Zeocin were purchased from Invitrogen. Geneticin was purchased from Gibco. Protease Inhibitor Cocktails were purchased from Roche. Water and organic solvents were purchased from Thermo Fisher Scientific. All other chemicals unless otherwise noted, were from Sigma–Aldrich or Wako.
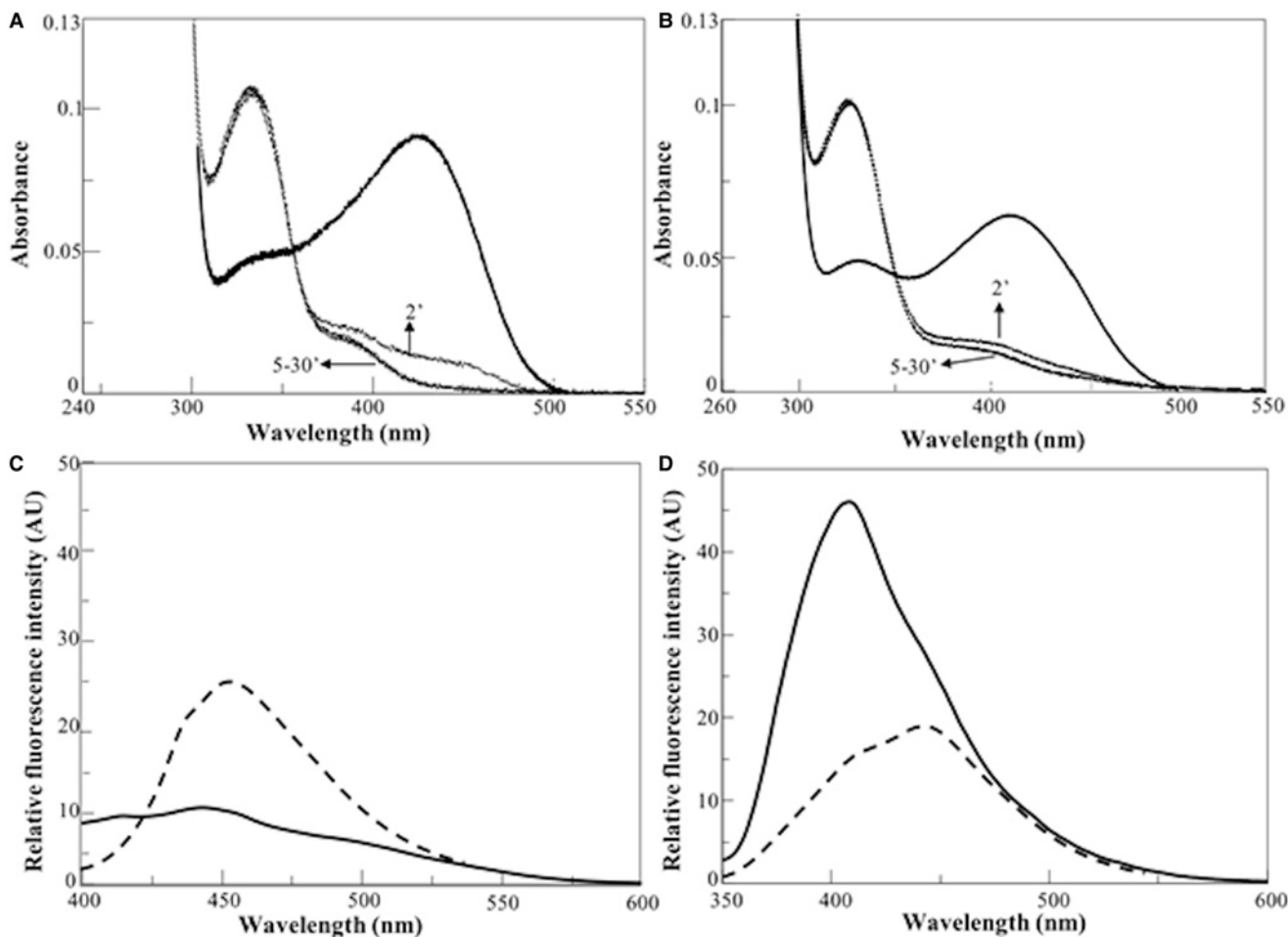
PORTLAND PRESS

Figure 1. Spectral changes and fluorescence spectra of AGT and the G41R variant upon addition of LCS.
(**A**) Time-dependent absorbance spectra of 9 μM wild-type AGT in the absence (black line) or in the presence of 100 μM LCS (dotted line) at the indicated times. (**B**) Time-dependent absorbance spectra of 9 μM G41R-Ma variant in the absence (black line) or in the presence of 100 μM LCS (dotted line) at the indicated times. (**C**) Fluorescence emission intensity upon excitation at 380 nm for wild-type AGT (—) and the G41R variant (—) at 1 μM protein concentration. (**D**) Fluorescence emission intensity upon excitation at 334 nm for wild-type AGT (—) and at 325 nm for the G41R variant (—) at 1 μM protein concentration. The experiments have been performed in KP 0.1 M pH 7.4 at 25°C.

AGT expression and purification

Escherichia coli BL21 cells were transformed with the constructs pAGThisMa and pAGThisG41R-Ma encoding the most common polymorphic form of AGT (major allele here called wild-type AGT) and the G41R variant on the background of the major allele, respectively. Expression and purification of the two proteins were performed as already reported [24].

Spectroscopic measurements

Absorbance spectra were registered using a Jasco V-750 spectrophotometer using 1 cm path length quartz cuvettes at a protein concentration of 0.1–20 μM in 0.1 M potassium phosphate buffer (KP), pH 7.4. Wild-type AGT and the G41R variant concentrations were determined using the previously determined molar absorption coefficient of 95 400 M^{-1} cm^{-1} at 280 nm [24]. PLP content was measured after treatment of the holoenzyme with 0.1 M NaOH using molar absorption coefficient of 6600 M^{-1} cm^{-1} of free PLP at 388 nm. Fluorescence data were obtained using 1 cm optical quartz cuvettes in a Jasco FP-8200 fluorimeter with excitation and emission bandwidths of 5 nm. All measurements were performed in KP 0.1 M pH 7.4.

Activity assays

To determine the kinetic parameters of the L-alanine/glyoxylate pair, purified proteins (0.1–0.2 μM) were incubated in the presence of 100 μM PLP in KP 0.1 M pH 7.4 at 25°C at increasing substrate concentrations and a fixed co-substrate concentration. The reaction was stopped by adding TCA 10% (v/v) and pyruvate production was measured using a spectrophotometric assay coupled with LDH [25]. Data were fitted to the Michaelis–Menten equation.

The AGT enzymatic activity in cell lysates was determined by incubating 100 μg of lysate with 0.5 M L-alanine and 10 mM glyoxylate in the presence of 100 μM PLP for 20 (wild-type AGT) or 50 (G41R variant) min in KP 0.1 M pH 7.4 at 25°C. Upon addition of TCA 10% (v/v), pyruvate production was measured using the spectrophotometric assay coupled with LDH.

Inhibition studies

The IC_{50} for LCS and DCS was determined by incubating each species in the presence of inhibitor at increasing concentrations (from 1 μM to 50 mM) and then measuring the residual transaminase activity. Each mixture contained 0.1 μM purified recombinant enzyme, 100 μM PLP, LCS or DCS, 10 mM glyoxylate, in KP 0.1 M pH 7.4. The reaction was started by the addition of 50 mM L-alanine.

The inhibition constant (K_I) of wild-type AGT and the G41R variant for LCS was determined by calculating the kinetic parameters for L-alanine at various LCS concentrations (from 50 to 400 μM) and by performing a global (shared-parameter) fitting of the data using a competitive inhibition model.

The slow-binding inhibition kinetics of DCS was evaluated using the progression curve method [26]. A solution of 0.1 μM wild-type AGT or 0.2 μM G41R variant in the presence of 100 μM PLP was added to reaction mixtures containing DCS (from 1 mM to 10 mM), L-alanine (250 mM), and glyoxylate (10 mM), in KP 0.1 M pH 7.4 and incubated at 25°C. At various times, aliquots were collected, the reaction was stopped by the addition of TCA 10% (v/v), and pyruvate produced was measured using LDH as coupled enzyme. Data for each progression curve were fitted to the integrated rate equation for slow binding inhibitors

$$[P] = v_s t + (v_0 + v_s)(1 - \exp(-k_{obs})/k_{obs}) \tag{1}$$

where, v_0 represent the initial rate, v_s the steady-state rate, k_{obs} the apparent first-order rate constant characterizing the formation of the steady-state enzyme–inhibitor complex. The obtained k_{obs} values were further analyzed for a one-step association mechanism

$$k_{obs}^{app} = k_{on}^{app}[I] + k_{off} \tag{2}$$

where, k_{off} and k_{on} are the dissociation and association rate constants, respectively. Intercept and slope values, obtained by linear regression of the k_{obs} versus inhibitor concentration plot (eqn 2), yielded the association and dissociation rate constants k_{on} and k_{off}, respectively, and the inhibition constant (eqn 3)

$$K_I^{app} = k_{off}/k_{on}^{app} \tag{3}$$

K_{on}^{app} was determined from the slope of the plot and then corrected for substrate competition using the equation

$$k_{on}^{true} = k_{on}^{app}\left(1 + \frac{[S]}{K_m}\right) \tag{4}$$

The K_I^{true} value was obtained from the equation

$$K_I^{true} = k_{off}/k_{on}^{true} \tag{5}$$

Crystallization and data collection

Crystallization of the AGT–DCS complex was attempted by co-crystallization using the vapor diffusion (hanging drop) technique: 1 µl of protein/ligand solution (215 µM AGT; 2 mM DCS; KP 50 mM pH 7.4) was mixed with an equal volume of reservoir: 10–12% PEG 6K; 5% 2-methyl-2,4-pentanediol (MPD); 0.1 M MES pH 6.5. Single crystals were cryoprotected by fast soaking into a reservoir solution containing 2 mM DCS and 25% MPD. For the AGT–LCS complex, AGT native crystals grown in the described conditions, with the exception of DCS, were soaked into a solution containing the reservoir and 20 mM LCS and 20% MPD, before flash freezing into $N_2(l)$ after 20 s. Complete data sets were collected at the ESRF in Grenoble on the ID23-1 beamline (operated by the MxCuBE [27] software) at 2.7 and 3.0 Å resolution for the AGT–DCS and AGT–LCS crystals, respectively. Data were indexed and integrated with XDS [28] and scaled with Aimless [29] within the CCP4 software suite [30]. Both crystals belonged to the $P4_12_12$ space group with one monomer in the asymmetric unit. Initial phases were obtained by molecular replacement using MOLREP [31] and 1.7 Å resolution structure of AGT as template (pdb: 5F9S [8]). Cycles of model building and refinement were performed with COOT [32] and REFMAC5 [33], respectively. The models geometry was validated with MolProbity [34] before deposition in the protein data bank with accession code 6RV0 and 6RV1 for the AGT–DCS co-crystallization and for the LCS soaked crystal, respectively. Data collection and refinement statistics are reported in Supplementary Table S1.

UPLC analyses

An amount of 10 µM AGT was inactivated in presence of 2 mM LCS or DCS at 25°C. After 2 h, the reactions were stopped by the addition of TCA 10% (v/v) and the samples were centrifuged at 18000**g** for 20 min followed by filtration using Millex-GV 0.22 µm filters (Merck MilliPore Ltd). Aliquots were analyzed by UPLC (Waters UPLC Acquity H class) using a Waters Cortecx C18+, 2.7 µm, 2.1 mm × 150 column equilibrated with 50 mM potassium phosphate pH 2.35 [35]. An isocratic elution was used for 6 min. Each injection was 3 µl with a flow rate of 0.2 ml/min and absorbance was monitored at 295 nm.

Mass spectrometry (MS)

To identify small molecule reaction products, AGT was inactivated with LCS or DCS as described for UPLC analyses, and each sample was deproteinized by TCA 10% (v/v). High-resolution mass spectra were recorded on a Thermo Scientific LTQ Orbitrap electrospray ionization (ESI) ion trap mass spectrometer. Sample volumes were typically 5 µl under automated injection into a LC system equipped with a C18 column followed by separation in a methanol : water (50 : 50) mobile phase. The mass spectrometer was set up in full scan mode, with a range from 150 to 2000 m/z and a resolution of 60 000.

To analyze the LCS- or DCS-inactivated AGT by MS, 10 µg of each protein sample were diluted in 100 µl of 50 mM ammonium bicarbonate, reduced with 10 mM dithiothreitol (Wako Co.) and then alkylated with 55 mM iodoacetamide (Wako Co.). Overnight digestion was done with Lys-C/Trypsin combo (Promega Co.) in a 1 : 50 enzyme : protein ratio. Upon stopping the digestion with 1% trifluoroacetic acid, the peptide mixture was cleaned with desalting C18 tips (StageTip, Thermo), vacuum-centrifuged to dryness, and re-suspended with 30 µl of 0.1% formic acid in water for LC/MS analysis. Data were collected using a Q-Exactive Plus mass spectrometer (ThermoFisher Scientific) coupled with Dionex Ultimate 3000RS liquid chromatography system (ThermoFisher Scientific). An analytical column Zorbax 300SC-18 0.3 × 150 mm, 3.5 µm (Agilent Co.) was used for sample chromatographic separation. Peptides were separated at a flow rate of 3.5 ml/min using a gradient of 1–42% ACN (0.1% formic acid) over 60 min.

Raw data files were searched against a composite target/decoy database using SEQUEST HT from Proteome Discoverer software (PD, v.2.2, Thermo Fisher Scientific). The *E. coli* protein database was downloaded from UniProt (UP000000625), combined with contaminants database (cRAP,https://www.thegpm.org/crap) and target protein sequence *AGXT* (Uniprot accession P21549). MS2 spectra were searched with ±20 ppm for precursor ion mass tolerance,±0.1 Da for fragment ion mass tolerance, using trypsin as enzyme, two missed cleavages maximum, dynamic modifications for oxidation of methionine and deamidation of glutamine and asparagine, fixed modification carbamidomethylation of cysteine residues and variable modification of lysine with PLP (mass shift +231.02911, C8H10NO5P). Label-free quantification based on peak intensity, using unique and razor peptides, and normalized using total protein amount. Extracted ion chromatogram (XIC) and isotopic ion distribution were done using Xcalibur software (ThermoFisher Scientific).

Docking studies

The crystal structure of human AGT (PDB ID: 1H0C) (7) has been protonated using the Protonate 3D tool of MOE 2018.0101 and the docking site was selected using the MOE Site Finder tool. LCS and DCS structures were docked into the active site of wild-type AGT using the MOE Dock tool. As a first step, Placement generates a collection of ligand conformations using the bond rotation method. These are then placed in the site by the Triangle Matcher method and ranked using the London dG scoring function, which estimates the free energy of binding of the ligand from a given pose. Finally, the Refinement tool is used for energy minimization of the pocket, before rescoring the poses with Affinity dG, which estimates the enthalpic contribution to the free energy of binding. The top 30 poses for each ligand were output in the MOE database and analyzed by visual inspection of the structure.

Cell culture and lysis

Chinese hamster ovary cells stably expressing glycolate oxidase (CHO-GO), and CHO-GO clones expressing wild-type AGT (CHO-GO-AGT-wt) or the G41R variant (CHO-GO-AGT-G41R), were cultured in Ham's F12 Glutamax medium supplemented with fetal bovine serum (10%, v/v), penicillin (100 units/ml) and strepto-mycin (100 μg/ml) at 37°C in a 5% CO_2 humidified environment. The expression of AGT and GO was maintained by adding G-418 (0.8 mg/ml) and Zeocin (0.4 mg/ml), respectively, to the culture medium. To test the effects of LCS or DCS, cells were cultured for 7 days in the absence or presence of one of the two CS enantiomers at 100 μM concentration. At the end of treatment, cells were harvested and lysed by freeze/thawing (five cycles) in Phosphate Buffer Saline (PBS), pH 7.2 supplemented with 100 μM PLP and protease inhibitor cocktail (Complete Mini, Roche). The whole-cell extract was separated by centrifugation (29,200**g**, 10 min, 4°C) to obtain the soluble fraction. Protein concentration in the soluble fraction was measured using the Bradford protein assay.

Western blot analyses

An amount of 5 μg of soluble cell lysate were loaded on 10% SDS–PAGE, transferred on a nitrocellulose membrane and immunoblotted with anti AGT antibody (1 : 10.000) in 2.5% (w/v) milk in TTBS (50 mM Tris–HCl, pH 7.5, 150 mM NaCl, 0.1% Tween 20) overnight at 4°C. After three washes in TTBS, the membrane was incubated with peroxidase-conjugated antirabbit immunoglobulin G (IgG) (1 : 10.000) in 5% milk in TTBS for 1 h at room temperature. Immunocomplexes were visualized by an enhanced chemiluminescence kit (ECL, Pierce Biotechnology, Rockford, IL).

Glycolate toxicity assay

CHO-GO, CHO-GO-AGT-wt, and CHO-GO-AGT-G41R cells were seeded in Petri dishes in Ham's F12 Glutamax medium. Where indicated, 100 μM DCS was added to the culture medium. After 6 days cells were detached and seeded in 96-well plates at a density of 8000 cells/well and exposed to 0.5 mM glycolate. After 24 h of treatment cell viability was assessed by crystal violet staining and results were normalized to that of controls grown without glycolate, as previously described [36].

Statistical analysis

Experiments have been performed at least in triplicate and in any case the standard error mean (SEM) was <10%. Statistical analyses were performed by Origin® 7 (Origin Lab) or GraphPad Prism Version 6.0 (GraphPad software, San Diego, CA, U.S.A.).

Results

Binding of LCS to wild-type and mutant AGT

We evaluated the interaction of LCS with wild-type AGT (encoded by the most common major allele) [37] and the G41R variant (on the background of the major allele) by absorbance spectroscopy. As previously reported, purified holoAGT displays an absorbance peak at 423 nm and a shoulder at ~340 nm corresponding to the oxoenamine and enolimine tautomers of the internal aldimine, respectively [1]. The addition of 100 μM LCS to wild-type AGT caused the disappearance of the band at 423 nm and the concomitant appearance of a peak at 334 nm, with a shoulder at 380 nm (Figure 1A). The same spectroscopic changes occurred upon LCS addition to the G41R variant, although in the mutant the band was centered at 325 nm (Figure 1B). Upon

excitation at 380 nm, the AGT–LCS and the G41R–LCS complexes showed a fluorescence emission spectrum with maximum at 450 nm, typical of the oxime formed between the ligand and PLP [38] (Figure 1C). On the other hand, the bands a 334 nm and at 325 nm produced a fluorescence emission at 408 nm and 416 nm for wild-type and mutant AGT, respectively (Figure 1D). These features are indicative of coenzyme forms with a C4′ showing sp³ hybridization [39]. Based on the known mechanisms of interaction of CS with PLP-enzymes, different hypotheses on the attribution of the 334 and 325 nm bands can be formulated. One of them is the formation of an inactive hydroxyisoxazole-PMP adduct, as previously reported for alanine racemase and branched-chain aminotransferase [14,15]. However, we found that the addition of the glyoxylate ketoacid to the enzyme–LCS complex led to the recovery of the ketoenamine tautomer of the internal aldimine (Supplementary Figure S1A). This suggests that the band is related to an active form of the coenzyme, such as PMP or a ketimine intermediate, which undergoes reverse half-transamination in the presence of an amino acceptor [5,22].

To gain structural details of the AGT–LCS complex, we crystallized wild-type holoAGT and we soaked the crystals into a solution containing LCS. We collected data at 3.0 Å resolution (Supplementary Table S1). In the omit map (Figure 2A) we observed a continuous electron density for the Schiff base bond between PLP and Lys209. After refinement of a model including the internal aldimine, the presence of a weak positive peak near the C4′ of PLP and the low density of the Lys209 side chain suggested the presence of a mixed situation. It
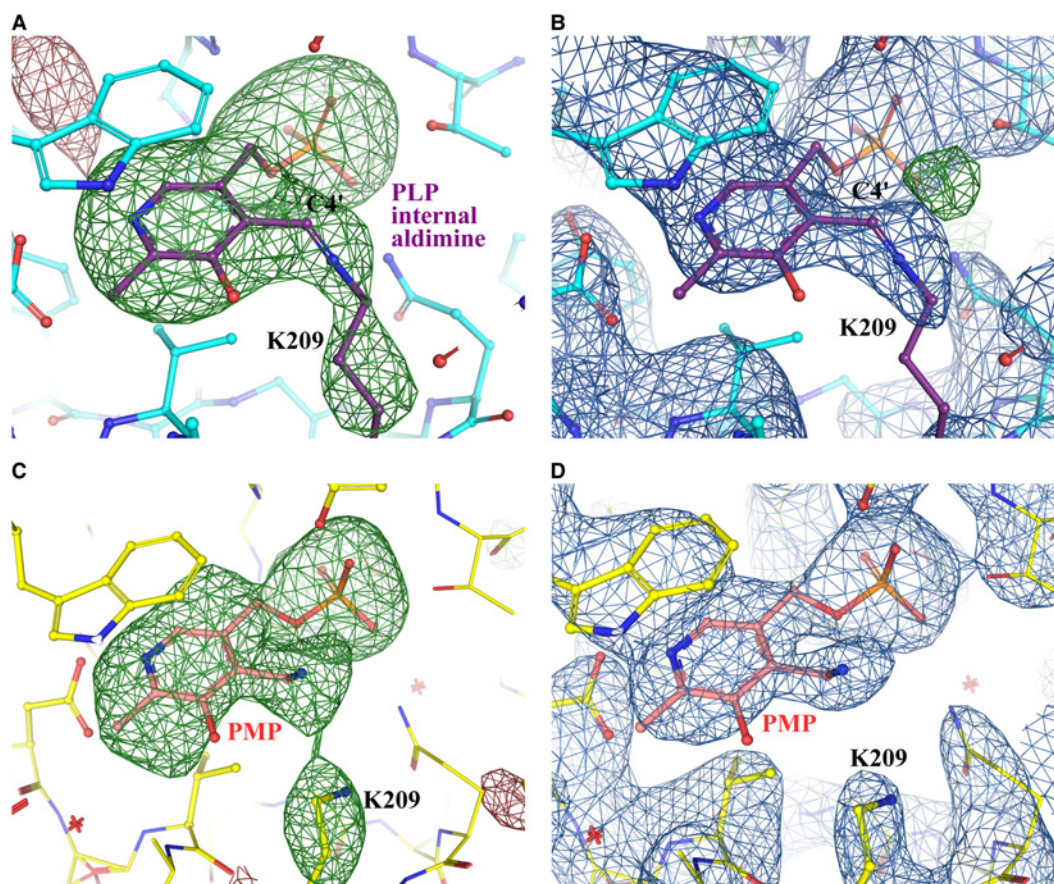

Figure 2. (A) Omit map showing the positive electron density (F_o–F_c map: in *green* contour level 3.0 sigma — 0.14 e/Å³) of the AGT crystal soaked with LCS. **(B)** Electron density maps after refinement of the final model including PLP internal aldimine (*purple*) with an occupancy of 0.75; $2F_o$–F_c map (contour 1.5 sigma) in *blue*. A small positive peak in the F_o–F_c map (in *green* contour level 3.0 sigma) is also observed near the PLP C4′ atom suggesting that a small amount of PMP may also be present in the active site. **(C)** Omit map showing the positive electron density (F_o–F_c map: in *green* contour level 3.0 sigma — 0.15 e/Å³) of the AGT–DCS co-crystallization crystal. Maps were calculated omitting K209, and PLP from the model. **(D)** Electron density maps after refinement of the final model including PMP (*pink*) with an occupancy of 0.75; $2F_o$–F_c map (contour 1.5 sigma) in *blue*.

Q4

must be clarified that the electron density maps represent the average state of the active site among all the proteins in the crystal. In this case the data suggest that, although the majority of the proteins display the internal aldimine at the active site, a small percentage of PMP may also be present in the crystal (Figure 2B). However, given the low resolution of these data, it was not possible to refine neither PMP nor a mixed model with both the internal aldimine and PMP at different occupancies in the active site, and the final model consisted of the internal aldimine with an occupancy of 0.75 (i.e. 75% of all the proteins of the crystal).

LCS inhibition mechanism

LCS led to a concentration-dependent drop in transaminase activity, confirming its role as inhibitor, with IC_{50} values of 50 μM and 136 μM for wild-type and G41R mutant AGT, respectively. Importantly, LCS inhibition was reversible, since the addition of L-alanine at saturating concentration to a preformed AGT–LCS complex caused an almost complete recovery (90%) of catalytic activity for both wild-type and variant. The IC_{50} value of both species did not change as a function of the incubation time (Supplementary Table S2), thus excluding the occurrence of a time dependent inhibition. Since LCS undergoes half-transamination, we hypothesized that it could be a competitive inhibitor for AGT. Indeed, the kinetic parameters of the enzymes for the substrate L-alanine indicate that the presence of LCS does not affect the value of V_{max}, while it causes a concentration-dependent increase in the K_M value. By a global fitting of the data we calculated K_i values of 37 ± 4 μM and 61 ± 10 μM for wild-type AGT and the G41R variant, respectively (Figure 3). It should be noted that the K_i value of the variant is 2-fold higher than that of the wild-type, in line with previous data showing that the Gly41 mutation induces slight changes of the AGT active site architecture [22].

Binding of DCS to wild-type and mutant AGT

The addition of 1 mM DCS to wild-type AGT caused a time-dependent disappearance of the absorbance bands at 420 and 340 nm and the concomitant appearance of an absorbance band at 370 nm (Figure 4A). The same band also appeared upon DCS addition to the G41R variant, although in this case an absorbance band at 331 nm was also present, suggesting the formation of two species (Figure 4B). The excitation at 370 nm of the two enzyme–DCS complexes generated a fluorescence emission spectrum with maximum at 450 nm, indicating the presence of an oxime intermediate (Figure 4C) [13]. On the other hand, the band at 331 nm of the variant could be ascribed either to the inactive enolimine tautomer of the internal aldimine, or to the formation of a ketimine intermediate.

We co-crystallized wild-type AGT in the presence of DCS at 2.5 Å resolution (Supplementary Table S2). Inspection of the electron density maps in the active site suggested the absence of the Schiff base bond between Lys209 and the C4′ of PLP (Figure 2C). Additional electron density on the opposite side of the C4′ atom further suggested that the internal aldimine had reacted with DCS. After several attempts the best fit for the observed electron density was PMP, which refined with reasonable B-factors and real space correlation coefficients (RSCC) values [38,40] when included in the model with a 0.75 occupancy (Figure 2D). Also in this case, from the density and B-factor analysis the presence of unreacted internal aldimine and/or apo active sites may not be excluded.

Inhibition mechanism mediated by DCS

Since the absorbance spectra evidenced a time dependent binding of DCS, we determined the IC_{50} upon incubation of the wild-type enzyme and the G41R variant with the inhibitor at different time points (20 min, 60 min and overnight) at 25°C. The values reported in Supplementary Table S2 show a decreasing IC_{50} value at increasing incubation time, a behavior consistent with time-dependent inhibition. Nevertheless, the addition of L-alanine at saturating concentration to a preformed AGT–DCS complex caused a time-dependent and almost complete recovery of catalytic activity, while the incubation of the wild-type AGT–DCS and G41R–DCS complexes with PLP alone led to a recovery of activity of 23% and 54%, respectively (Supplementary Figure S2). These data indicate that DCS inhibition can be completely reversed by the substrate but not by the coenzyme, thus suggesting that the ligand does not form an irreversibly modified coenzymatic form as reported for other enzymes of the same family [14,15].

To better investigate the mechanism underlying the time-dependent inhibition mediated by DCS, we determined the progression curves of the loss of enzymatic activity as a function of time in the presence of the inhibitor at increasing concentrations (Figure 5A–C). For each curve we calculated the k_{obs} using equation 4. It should be considered that there are two common mechanisms of slow-binding inhibition. The first, called
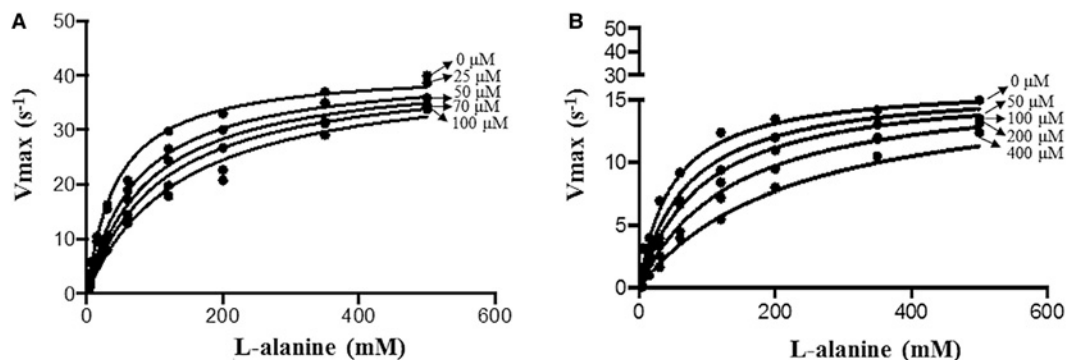
Figure 3. Determination of kinetic parameters of wild-type AGT and the G41R variant for L-alanine in presence of LCS.
(**A**) Cumulative fitting of kinetic parameters of AGT-Ma for L-alanine in absence or presence of LCS at the indicated micromolar concentrations (eqn 3). (**B**) Cumulative fitting of kinetic parameters of the G41R variant vs L-alanine in absence or presence of LCS at the indicated micromolar concentrations (eqn 3). Experiments have been performed in KP 0.1 M pH 7.4 at 25°C.
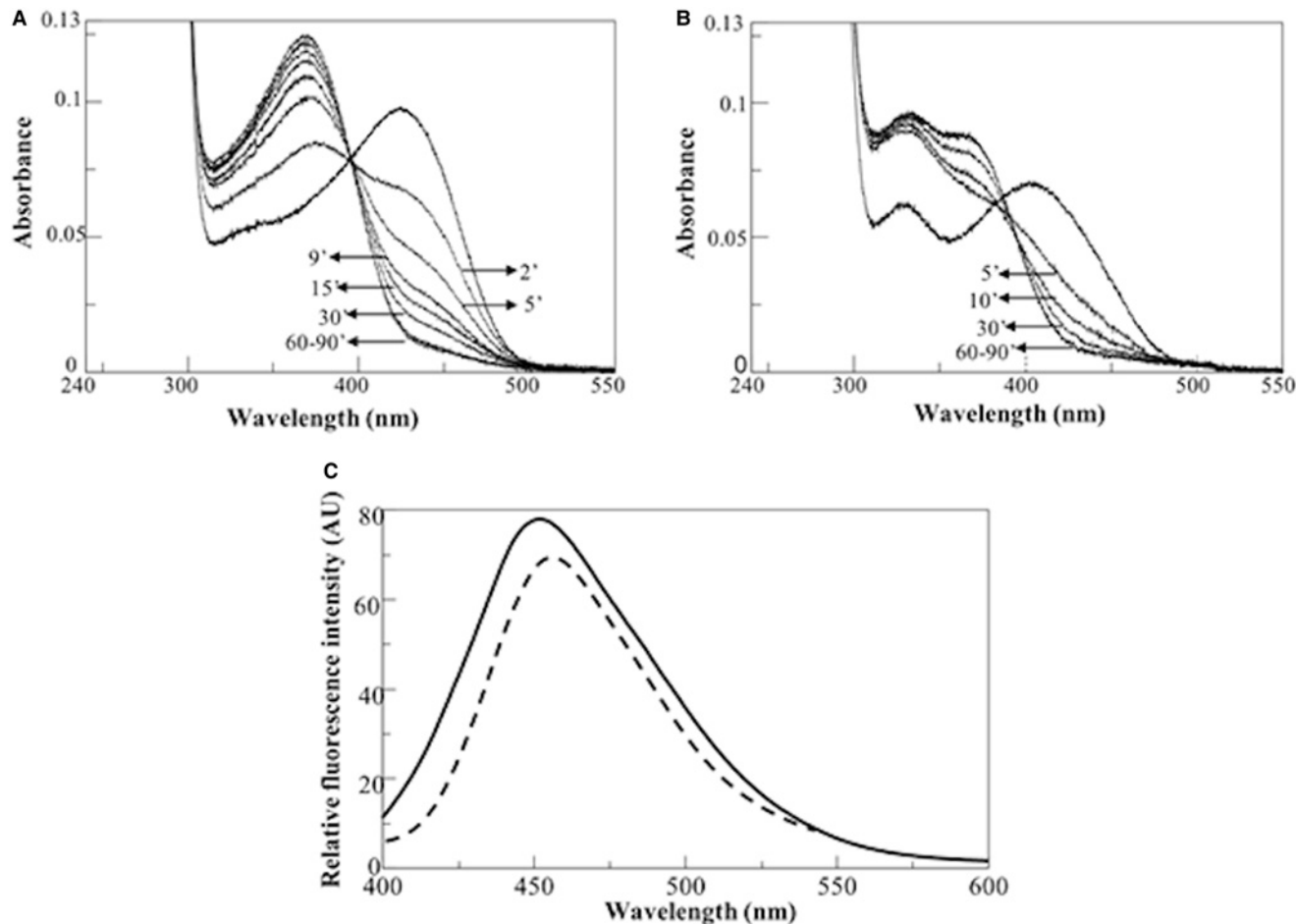

Figure 4. Spectral changes and fluorescence emission spectra of wild-type AGT and the G41R variant upon addition of DCS.
(**A**) Time-dependent absorbance spectra of 9 µM wild-type AGT in the absence (black line) or in the presence of 1 mM DCS (dotted lines) at the indicated times. (**B**) Time-dependent absorbance spectra of 9 µM G41R in the absence (black line) or in the presence of 5 mM DCS (dotted lines) at the indicated times. (**C**) Fluorescence emission spectra of 1 µM wild-type AGT (—) and of the G41R variant (—) in complex with DCS upon excitation at 370 nm. Experiments have been performed in KP 0.1 M pH 7.4 at 25°C.
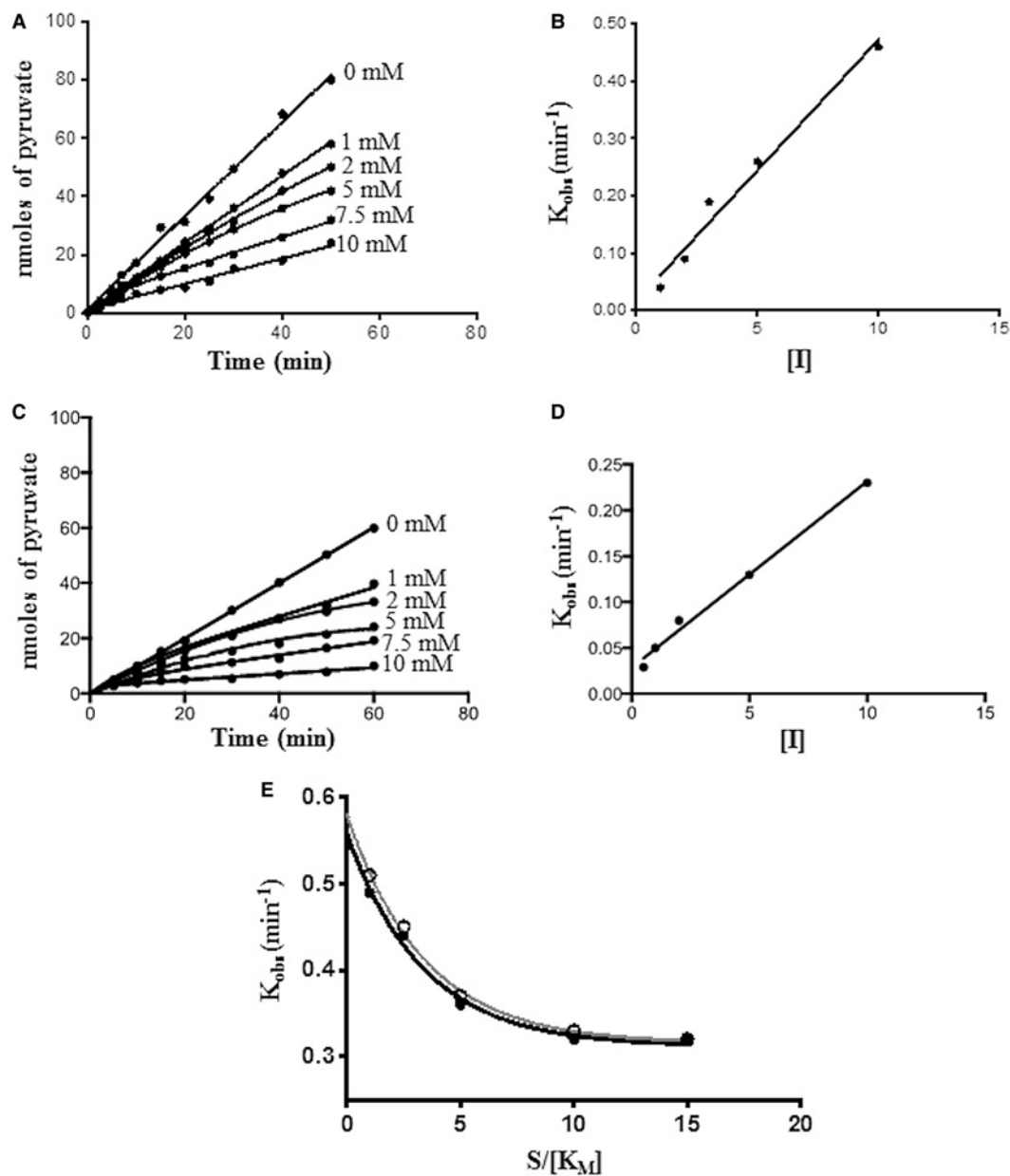
Figure 5. Time dependent inhibition of wild-type AGT and the G41R variant by DCS.
(**A**) Progression curves of wild-type AGT (0.1 μM) in the presence of the indicated concentrations of DCS in KP 0.1 M pH 7.4 at 25°C. (**B**) Trends of the k_{obs} values obtained using equation 4 as a function of inhibitor concentration. (**C**) Progression curves of the G41R variant (0.2 μM) in the presence of the indicated concentrations of DCS in KP 0.1 M pH 7.4 at 25°C. (**D**) Trends of the k_{obs} values obtained using equation 4 as a function of inhibitor concentration. (**E**) Trends of the k_{obs} values for wild-type AGT (closed symbols) and G41R (open symbols) obtained at 0.1 μM enzyme concentration in the presence of 5 mM DCS, at increasing substrate concentration (30–500 mM).

'one-step slow binding inhibition', is described by the scheme: $E + I \leftrightarrow EI$ and involves the direct formation of an inactive enzyme-inhibitor complex. The second, called 'two-step slow binding inhibition' or 'isomerization slow binding inhibition', is described by the scheme: $E + I \leftrightarrow EI \leftrightarrow EI^\star$ and involves the formation of the enzyme–inhibitor complex followed by an isomerization generating an inactive complex. To distinguish between the two models, we plotted the apparent first-order rate constant (k_{obs}) against inhibitor concentration. As reported in Figure 5B,D, for both wild-type AGT and the G41R variant we observed a linear trend,

Table 1. Kinetic constants of the time-dependent inhibition of DCS for wild-type AGT and the G41R variant

Enzyme	k_{on} (mM^{-1} min^{-1})	k_{off} (min^{-1})	K_I^{true} (μM)
Wild-type	$9.1 \pm 0.4 \times 10^{-2}$	$1.6 \pm 0.2 \times 10^{-2}$	175 ± 23
G41R	$4.1 \pm 0.2 \times 10^{-2}$	$2.8 \pm 0.5 \times 10^{-2}$	682 ± 134

indicating that the reaction kinetics follows a one-step slow-binding inhibition mechanism. From the linear fit of the data to equation 5, we calculated the association and dissociation rate constants, and then the apparent enzyme–DCS equilibrium dissociation constants (K_I^{app}). To define the modality by which the inhibitor interacts with the enzyme, we determined the k_{obs} values from progression curves obtained at a fixed saturating concentration of DCS in the presence of increasing concentrations of the substrate. As shown in Figure 5E, the k_{obs} values decrease as substrate concentration increases. This trend is indicative of a competitive inhibition and allows to calculate the true K_I values from the K_I^{app}. The kinetic constants describing DCS inhibition are summarized in Table 1.

Identification of the wild-type and mutant AGT-cycloserine reaction products

To exclude the occurrence of covalent modifications upon interaction with CS, we performed MS analyses after limited proteolysis of AGT samples before and after inactivation by LCS or DCS. As expected, the results confirmed the presence of a covalent PLP–Lys209 complex in the untreated sample. The same complex was also present in the AGT–LCS and AGT–DCS sample, although its relative abundance was 7% and 29%, respectively, as compared with untreated AGT (Supplementary Figure S3), as expected considering that the internal aldimine is converted to other reaction intermediates upon reaction with CS (see below). Thus, AGT inhibition was not due to the covalent modification of any active site residue.

We then performed UPLC analyses to determine the changes in coenzyme content using a previously setup method [35]. As reported in Figure 6A, upon reaction with LCS 77% of the initial PLP content of AGT is converted to PMP, in agreement with what observed in the presence of L-alanine and confirming the occurrence of an half-transamination. On the other hand, upon reaction with DCS only 4% of PLP was converted to PMP, while 24% eluted as unmodified PLP and the remaining portion eluted as unidentified small peaks appearing at elution volumes higher than that of PLP. Notably, upon addition of L-alanine to the AGT–DCS complex, 80% of the coenzyme is converted to PMP. This further confirms that DCS forms a reversible complex with AGT, which can be displaced by the substrate. We then analyzed the AGT–DCS reaction products by ESI–MS (Figure 6B). We found (i) peaks at *m/z* 330.77 and 332.81, which can be attributed to the PLP–DCS external aldimine, or to a ketimine intermediate generated by a 1,3-prototropic shift, and (ii) peaks at *m/z* 348.78 and 350.78, which are compatible with the addition of a water molecule to the external aldimine complex leading to opening of the CS ring. The latter peaks could be ascribed to the external aldimine of PLP with formed β-aminoserine, an oxime generated by intramolecular rearrangement, or a ketimine between PMP and β-aminooxypyruvate [17,41]. Our spectroscopic and crystallographic data, along with the reversibility of the AGT inhibition process, allow to exclude the formation of a covalent PMP-isoxazole complex [14]. Moreover, no PMP formation is seen by UPLC, thus excluding the occurrence of an half-transamination. Thus, we can attribute the peaks at *m/z* 348.78 and 350.78 to an oxime intermediate.

We obtained a qualitatively similar ESI–MS pattern by analyzing the AGT–LCS reaction mixture, although in this case the intensity of the peaks at *m/z* 348.78 and 350.78 was lower than that obtained in the AGT–DCS sample (data not shown). It should be noticed that the obtained *m/z* values differ by 0.7 D from the expected values of the nominal mass of the PLP-CS complexes, probably due to already reported random errors that affect accuracy giving bias in mass measurements [42].

Effects of CS enantiomers on specific activity and expression level of wild-type AGT and the G41R variant in CHO-GO cells

To test if LCS and/or DCS could act as PCs for AGT variants showing folding defects, we took advantage of a cellular model made up of CHO cells that overexpress glycolate oxidase (CHO-GO) and recapitulate hepatic glyoxylate metabolism [43]. In the presence of glycolate in the culture medium, these cells produce glyoxylate
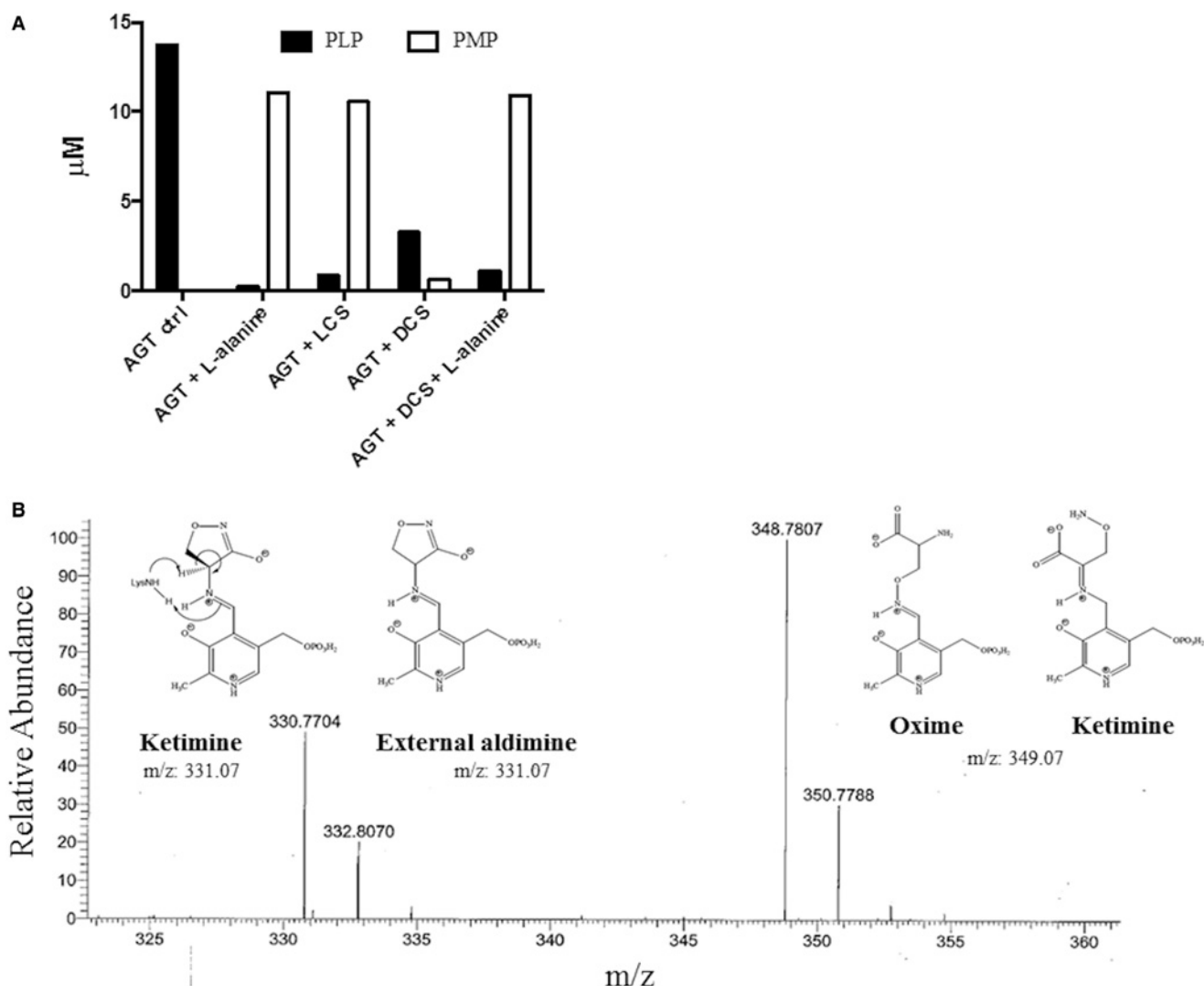
Figure 6. UPLC and ESI–MS analysis of AGT–CS reaction products.

(**A**) Coenzyme content of wild-type AGT upon 2 h reaction with 2 mM LCS or DCS at 25°C, as obtained by UPLC analysis. The reaction of the enzyme with saturating ʟ-alanine was used as positive control. (**B**) ESI–MS analysis of the wild-type AGT–DCS reaction mixture. The chemical structures attributed to each peak are shown. See the text for details.

inside peroxisomes and show a strongly reduced viability. CHO-GO cells stably transformed with wild-type AGT (CHO-GO-AGT-wt) or the G41R variant (CHO-GO-AGT-G41R) were grown in the presence or in the absence of 100 μM LCS or DCS in the culture medium for 7 days. CS concentration was chosen taking into account the inhibition constant values, and the use of a pharmacologically relevant ligand concentration, while the treatment time was that sufficient to allow protein synthesis and folding in the presence of the treating agent, considering the AGT half-life [44]. Upon cell harvesting and lysis, the soluble fraction of the lysate was used for experiments aimed at measuring the AGT expression level and specific activity. We found that neither LCS nor DCS alter the transaminase specific activity and the AGT expression level of CHO-GO-AGT-wt cells (Figure 6). As for the G41R variant, data obtained with the purified protein indicate that it displays an enzymatic activity corresponding to ∼10% that of wild-type AGT (in terms of k_{cat}). When expressed in CHO-GO cells, the variant showed 10% specific activity and 8% expression level in the soluble fraction, as compared with the wild type. These data confirm that the variant is endowed with a folding defect that reduces the amount of soluble and active protein present in the cell, in line with previous evidences indicating a higher tendency to aggregation induced by the Gly41 mutation [22]. Notably, LCS did not affect the specific activity and the

expression level of the variant. Since LCS undergoes half-transamination, we also tested the chaperone effect upon replenishment of LCS in the medium every 24 h. However, we did not notice any change in AGT expression or activity. On the other hand, DCS induced a statistically significant increase in specific activity (Figure 7A). To understand whether DCS-induced enhancement of enzymatic activity was dependent on an increased expression, we analyzed the protein levels CHO-GO-AGT-G41R cells (Figure 7B) and we found that DCS treatment mildly increases the amount of AGT present in the soluble fraction. These data suggest that the increased AGT specific activity of CHO-GO-AGT-G41R cells treated with DCS might depend on the capacity of this enantiomer to specifically bind the misfolded variant and improve its folding efficiency. In agreement with these results, the treatment with DCS significantly improved the glyoxylate detoxification ability of CHO-GO cells expressing the G41R variant (Figure 7C), because it increases cell viability upon glycolate treatment. These data confirm that the treatment increases the amount of intraperoxisomal functional AGT able to metabolize glyoxylate.

Discussion

This work is focused on the analysis of the interaction of AGT, a clinically relevant enzyme involved in the rare disorder PH1, with the two enantiomers of CS. We performed a spectral, kinetic, and structural characterization of the interaction of LCS and DCS with the purified enzyme both in the wild-type form encoded by the major allele and in a mutant form bearing a folding defect (G41R) on the background of the major allele [22]. We also tested the possible action of LCS and DCS as PCs, i.e. their ability to counteract the effects of the G41R pathogenic mutation in a cellular model.

Our results indicate that both LCS and DCS do not covalently modify AGT, but bind at the active site and reversibly inhibit transaminase activity in a competitive way. However, they show a different binding kinetics and generate a different equilibrium of species. Spectral and kinetic studies agree with LCS behaving as a classical competitive inhibitor that instantaneously undergoes transamination producing a ketimine and a small fraction of an oxime intermediate. Crystallographic data are in agreement with the occurrence of a half-transamination, although we did not obtain other clues about the product(s) and intermediates of the reaction. Since the AGT crystals were soaked with LCS, it must be considered that the reactivity in the crystal form is lower with respect to that in solution due to the slower diffusion of the ligand within the crystal lattice. Therefore, the reaction could have been incomplete, but longer soaking times resulted in non-diffracting crystals. Nevertheless, the UPLC analysis of the coenzyme content upon acidic deproteinization clearly confirms the formation of PMP, and ESI–MS data show a peak compatible with a ketimine intermediate.

On the other hand, DCS shows a time-dependent binding to wild-type AGT and to the G41R mutant, leading to spectral changes consistent with the formation of an oxime intermediate associated with the loss of catalytic activity. The kinetic analysis of the inhibition indicates that it follows a single-step competitive mechanism. It is not easy to explain why we did not detect the oxime intermediate in the crystal structure of the AGT–DCS complex, but we can speculate that it could undergo hydrolysis during the crystallization process or even radiation damage, as previously reported for other PLP intermediates [8]. UPLC and ESI–MS data confirm the reversibility of DCS binding and are consistent with the formation of an oxime generated by water addition to the isoxazolidone ring, followed by intramolecular rearrangement.

Overall, the mechanism that best recapitulates the results on the reaction of AGT with LCS or DCS is reported in Figure 8. The enzyme in the PLP-form reacts with LCS or DCS forming an external aldimine. In the case of LCS, a ketimine is formed upon direct deprotonation at Cα and reprotonation at the coenzyme C4′. However, it cannot be excluded that the 1,3-prototropic shift occurs on the external aldimine intermediate formed upon water addition to the CS ring. Molecular docking analyses of the AGT–LCS complex (Supplementary Figure S4) indicate that LCS is mainly held in place through a ring stacking interaction with Tyr260 of the neighboring subunit, and by hydrogen bonds between the exocyclic oxygen and Arg360. Notably, Lys209 is at 3.5 Å from Cα, thus in a favorable position to perform the 1,3-prototropic shift leading to ketimine formation. In the case of the AGT–DCS complex, the ligand moiety assumes a different conformation, with the amino group and the exocyclic oxygen interacting with Arg360. Thus, transaldimination is less favored, in agreement with the slow kinetics of DCS binding. Moreover, Lys209 is not properly positioned to act as acid/base catalyst, thus explaining why the AGT–DCS complex undergoes a ring-opening process mediated by water addition, a process probably favored by the liberation of the carboxylate group that can preferentially interact with Arg360. The latter step generates an intermediate that undergoes an intramolecular rearrangement producing an oxime of PLP with β-aminooxyserine [7].
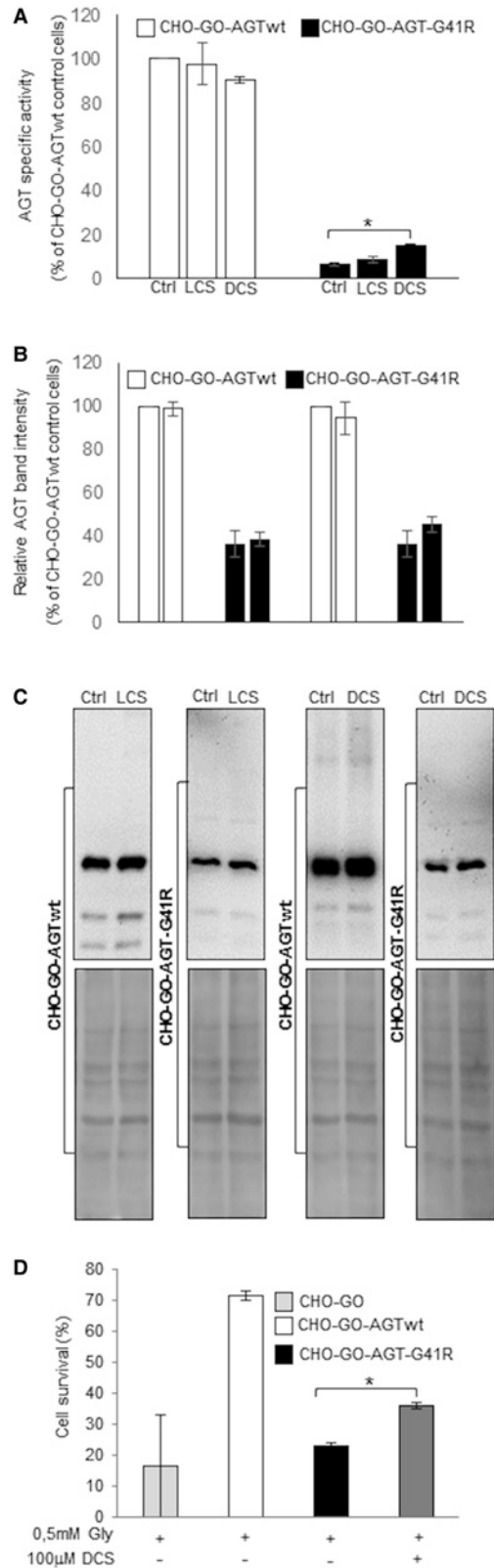
703
704
705
706
707
708
709
710
711
712
713
714
715
716
717
718
719
720
721
722
723
724
725
726
727
728
729
730
731
732
733
734
735
736
737
738
739
740
741
742
743
744
745
746
747
748
749
750
751
752
753
754
755
756

Figure 7. Effects of LCS or DCS treatment on specific activity and expression level of AGT. Part 1 of 2

CHO-GO-AGT-wt and CHO-GO-AGT-G41R cells were grown for 7 days in the presence or in the absence of 100 μM LCS or DCS. At the end of treatment cells were detached, lysed and soluble fraction of each sample used for: (**A**) AGT enzymatic

Figure 7. Effects of LCS or DCS treatment on specific activity and expression level of AGT. Part 2 of 2

activity determination. Specific activity of AGT in CHO-GO-AGT-wt control cells (192.54 ± 12.68 nmoles of pyruvate/min/mg protein) was assumed as 100%. Data represent mean ± SEM ($n = 4$). * $P < 0.005$, Student's t-test; (**B**) AGT expression level quantification. AGT levels in CHO-GO-AGT-wt control cells was assumed as 100%. (**C**) Representative western blot of AGT expression levels in the indicated cells clones. For each gel, the corresponding Ponceau staining of the total lysate is also shown as loading control. (**D**) Indirect glycolate toxicity assay. Histogram representative of cell viability after 24 h of treatment with 0.5 mM glycolate expressed as percentage with respect to untreated cells. Six replicates have been measured for each sample. CHO-GO and CHO-GO-AGT-wt cells represent the negative and positive control, respectively. The images are representative of one out of three separate experiments. Data represent mean ± SEM ($n = 4$).

The mechanism here described also explains why we noticed that both LCS and DCS are reversible inhibitors of AGT, as demonstrated by the recovery of activity in the presence of saturating concentrations of the physiological substrate L-alanine. LCS behaves as a classical competitive inhibitor, and thus can be displaced by the substrate when it is present at saturating concentration in the overall transamination reaction mixture. In addition, the ketimine formed with LCS is supposed to be in equilibrium with the external aldimine intermediate, thus explaining the recovery of activity when the AGT–LCS complex is preformed. A similar behavior has been already reported for competitive inhibitors of alpha-galactosidase A in Fabry disease [45,46] as well as for iminosugar derivatives as glucocerebrosidase inhibitors in Gaucher disease [47,48]. As for the oxime intermediate generated with DCS, it is not difficult to hypothesize that the α-amino group of L-alanine could compete with the N atom of ligand moiety for the binding to the C4′ of PLP and displace the inhibitor, thus leading to a recovery of catalytic activity. These findings get a new light on the mechanism underlying the action of LCS and DCS, because both molecules have been always considered as irreversible inhibitors of PLP-enzymes [15,49]. However, it should be pointed out that experiments aimed at testing the regain of activity induced by the substrate have not been performed in all previous studies.
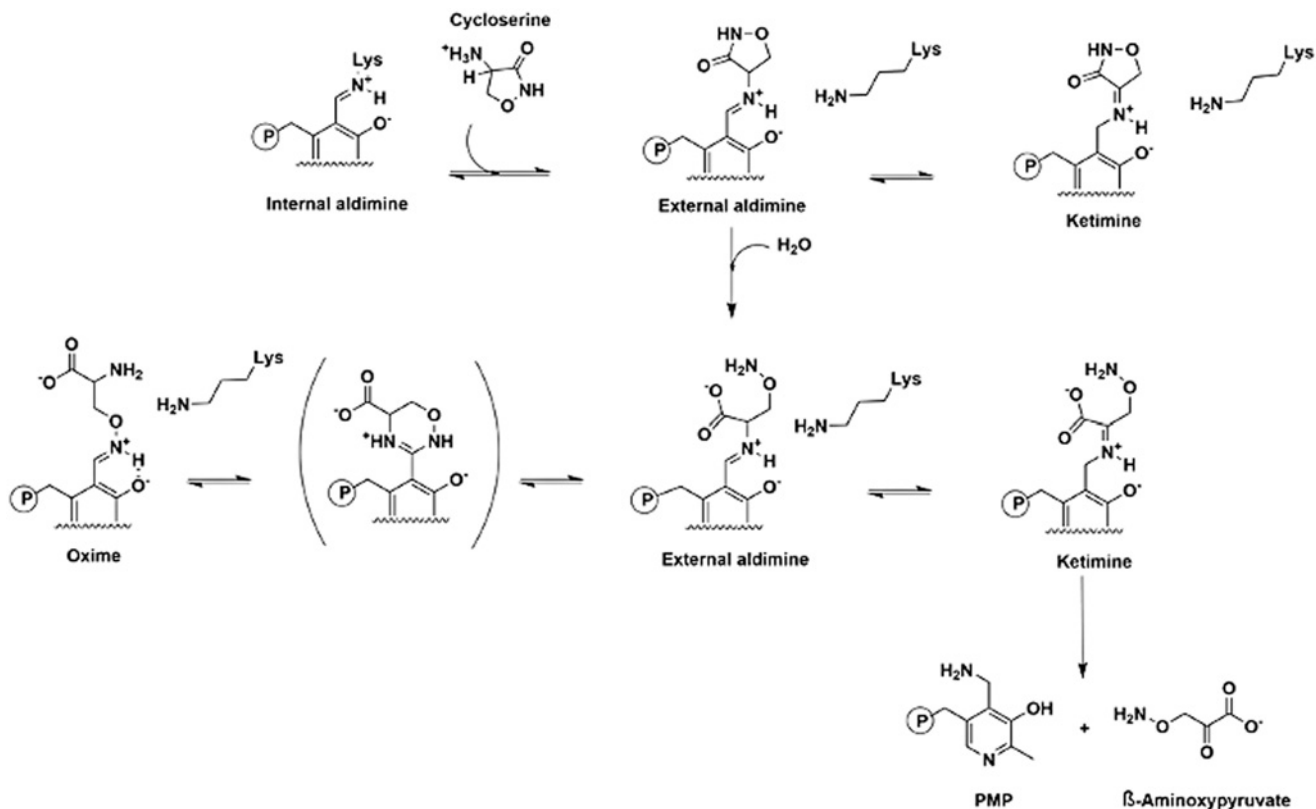

Figure 8. Proposed reaction mechanism of AGT with LCS or DCS.

The reversible behavior of LCS and DCS prompted us to test their action as PCs in a cellular model recapitulating the metabolic alterations typical of patients affected by PH1, a disease where misfolding is one of the main factors underlying the effects of pathogenic mutations in AGT. We used as models cells expressing wild-type AGT and cells expressing the G41R variant, which shows a folding defect giving rise to an increased tendency to aggregation and to intracellular degradation [22,23]. We found that only DCS is able to partly rescue for the pathogenic G41R mutation, leading to a recovery of catalytic activity paralleled by an increased portion of protein present in the soluble fraction. This can be understood considering that LCS behaves as a substrate, generating PMP, which can rapidly dissociate from the G41R variant inside the cell. On the other hand, the slow binding of DCS could allow the ligand to remain bound at the active site for a time long enough to promote the correct folding of the protein. It should be mentioned that DCS is a natural product used to treat resistant *Mycobacterium tuberculosis* infections as well as neurological disorders since it is a potent NMDA receptor agonist [50]. These findings strongly support the use of DCS as a valuable template for the synthesis of PCs for PH1. The preparation and biological evaluation of improved analogs is currently ongoing in our laboratories.

Abbreviations

2,4-DNP, 2,4-dinitrophenylhydrazine; AGT, alanine:glyoxylate aminotransferase; CS, cycloserine; DCS, D-cycloserine; ESI, electrospray ionization; KP, potassium phosphate buffer; LCS, L-cycloserine; LDH, L-lactate dehydrogenase; MPD, 2-methyl-2,4-pentanediol; MS, mass spectrometry; PBS, phosphate-buffered saline; PC, pharmacological chaperone; PH1, primary hyperoxaluria type 1; PLP, pyridoxal 5′-phosphate; PMP, pyridoxamine 5′-phosphate.

Authors contribution

M.D., S.G., G.C., M.P., B.C.: conceived and designed the experiments. M.D., S.G., G.A., G.G., G.P., A.F.: performed the experiments and analyzed the data. M.P., G.G., F.C., G.C., P.L.: analyzed the data and provided support for mass spectrometry and crystallography experiments. M.D., S.G., B.C. wrote the paper. All authors proof read and approved the manuscript.

Funding

Acknowledgements

Competing Interests

The Authors declare that there are no competing interests associated with the manuscript.

References

1   Cellini, B., Bertoldi, M., Montioli, R., Paiardini, A. and Borri Voltattorni, C. (2007) Human wild-type alanine:glyoxylate aminotransferase and its naturally occurring G82E variant: functional properties and physiological implications. *Biochem. J.* **408**, 39–50 https://doi.org/10.1042/BJ20070637
2   Cochat, P. and Rumsby, G. (2013) Primary hyperoxaluria. *N. Engl. J. Med.* **369**, 649–658 https://doi.org/10.1056/NEJMra1301564
3   Hoppe, B. (2012) An update on primary hyperoxaluria. *Nat. Rev. Nephrol.* **8**, 467–475 https://doi.org/10.1038/nrneph.2012.113
4   Cochat, P., Fargue, S. and Harambat, J. (2010) Primary hyperoxaluria type 1: strategy for organ transplantation. *Curr. Opin. organ Transplant.* **15**, 590–593 https://doi.org/10.1097/MOT.0b013e32833e35f5
5   Dindo, M., Conter, C., Oppici, E., Ceccarelli, V., Marinucci, L. and Cellini, B. (2019) Molecular basis of primary hyperoxaluria: clues to innovative treatments. *Urolithiasis* **47**, 67–78 https://doi.org/10.1007/s00240-018-1089-z
6   Hoyer-Kuhn, H., Kohbrok, S., Volland, R., Franklin, J., Hero, B., Beck, B.B. et al. (2014) Vitamin B6 in primary hyperoxaluria I: first prospective trial after 40 years of practice. *Clin. J. Am. Soc. Nephrol.* **9**, 468–477 https://doi.org/10.2215/CJN.06820613
7   Zhang, X., Roe, S.M., Hou, Y., Bartlam, M., Rao, Z., Pearl, L.H. et al. (2003) Crystal structure of alanine:glyoxylate aminotransferase and the relationship between genotype and enzymatic phenotype in primary hyperoxaluria type 1. *J. Mol. Biol.* **331**, 643–652 https://doi.org/10.1016/S0022-2836(03)00791-5

8   Giardina, G., Paiardini, A., Montioli, R., Cellini, B., Voltattorni, C.B. and Cutruzzola, F. (2017) Radiation damage at the active site of human alanine:
     glyoxylate aminotransferase reveals that the cofactor position is finely tuned during catalysis. *Sci. Rep.* **7**, 11704 https://doi.org/10.1038/
     s41598-017-11948-w

9   Mandrile, G., van Woerden, C.S., Berchialla, P., Beck, B.B., Acquaviva Bourdain, C., Hulton, S.A. et al. (2014) Data from a large European study
     indicate that the outcome of primary hyperoxaluria type 1 correlates with the AGXT mutation type. *Kidney Int.* **86**, 1197–1204 https://doi.org/10.1038/
     ki.2014.222

10   Oppici, E., Montioli, R. and Cellini, B. (2015) Liver peroxisomal alanine:glyoxylate aminotransferase and the effects of mutations associated with primary
     hyperoxaluria type I: an overview. *Biochim. Biophys. Acta* **1854**, 1212–1219 https://doi.org/10.1016/j.bbapap.2014.12.029

11   Pey, A.L., Albert, A. and Salido, E. (2013) Protein homeostasis defects of alanine-glyoxylate aminotransferase: new therapeutic strategies in primary
     hyperoxaluria type I. *BioMed. Res. Int.* **2013**, 687658 https://doi.org/10.1155/2013/687658

12   Leidenheimer, N.J. (2018) Pharmacological chaperones: beyond conformational disorders. *Handb. Exp. Pharmacol.* **245**, 135–153 https://doi.org/10.
     1007/164_2017_68

13   Oppici, E., Montioli, R., Dindo, M., Maccari, L., Porcari, V., Lorenzetto, A. et al. (2015) The chaperoning activity of amino-oxyacetic acid on
     folding-defective variants of human alanine:glyoxylate aminotransferase causing primary hyperoxaluria type I. *ACS Chem. Biol.* **10**, 2227–2236
     https://doi.org/10.1021/acschembio.5b00480

14   Amorim Franco, T.M., Favrot, L., Vergnolle, O. and Blanchard, J.S. (2017) Mechanism-based inhibition of the *Mycobacterium tuberculosis*
     branched-chain aminotransferase by d- and l-cycloserine. *ACS Chem. Biol.* **12**, 1235–1244 https://doi.org/10.1021/acschembio.7b00142

15   Fenn, T.D., Stamper, G.F., Morollo, A.A. and Ringe, D. (2003) A side reaction of alanine racemase: transamination of cycloserine. *Biochemistry* **42**,
     5775–5783 https://doi.org/10.1021/bi027022d

16   Gregory, T., Olson, M.F., Lau, S., Rinehart, K.L. and Silverman, R.B. (1998) An aromatization mechanism of inactivation of γ-aminobutyric acid
     aminotransferase for the antibiotic L-cycloserine. *J. Am. Chem. Soc.* **120**, 12 https://doi.org/10.1021/ja971047w

17   Lowther, J., Yard, B.A., Johnson, K.A., Carter, L.G., Bhat, V.T., Raman, M.C. et al. (2010) Inhibition of the PLP-dependent enzyme serine
     palmitoyltransferase by cycloserine: evidence for a novel decarboxylative mechanism of inactivation. *Mol. Biosyst.* **6**, 1682–1693 https://doi.org/10.
     1039/c003743e

18   Prosser, G.A. and de Carvalho, L.P. (2013) Reinterpreting the mechanism of inhibition of *Mycobacterium tuberculosis* D-alanine:D-alanine ligase by
     D-cycloserine. *Biochemistry* **52**, 7145–7149 https://doi.org/10.1021/bi400839f

19   Ringe DPMCWVOMM. (1998) d-cycloserine inactivation of d-amino acid aminotransferase leads to a stable noncovalent protein complex with an
     aromatic cycloserine-PLP derivative. *J. Am. Chem. Soc* **120**, 7 https://doi.org/10.1021/ja972993f

20   Goff, D.C. (2017) D-cycloserine in schizophrenia: new strategies for improving clinical outcomes by enhancing plasticity. *Curr. Neuropharmacol.* **15**,
     21–34 https://doi.org/10.2174/1570159X14666160225154812

21   Williams, R.D., Sgoutas, D.S., Zaatari, G.S. and Santoianni, R.A. (1987) Inhibition of serine palmitoyltransferase activity in rabbit aorta by L-cycloserine.
     J. Lipid Res. **28**, 1478–1481 PMID:3430071

22   Cellini, B., Montioli, R., Paiardini, A., Lorenzetto, A., Maset, F., Bellini, T. et al. (2010) Molecular defects of the glycine 41 variants of alanine glyoxylate
     aminotransferase associated with primary hyperoxaluria type I. *Proc. Natl Acad. Sci. U.S.A.* **107**, 2896–2901 https://doi.org/10.1073/pnas.
     0908565107

23   Fargue, S., Lewin, J., Rumsby, G. and Danpure, C.J. (2013) Four of the most common mutations in primary hyperoxaluria type 1 unmask the cryptic
     mitochondrial targeting sequence of alanine:glyoxylate aminotransferase encoded by the polymorphic minor allele. *J. Biol. Chem.* **288**, 2475–2484
     https://doi.org/10.1074/jbc.M112.432617

24   Cellini, B., Montioli, R., Bianconi, S., Lopez-Alonso, J.P. and Voltattorni, C.B. (2008) Construction, purification and characterization of untagged human
     liver alanine-glyoxylate aminotransferase expressed in *Escherichia coli.* *Protein Pept. Lett.* **15**, 153–159 https://doi.org/10.2174/092986608783489580

25   Cellini, B., Lorenzetto, A., Montioli, R., Oppici, E. and Voltattorni, C.B. (2010) Human liver peroxisomal alanine:glyoxylate aminotransferase: different
     stability under chemical stress of the major allele, the minor allele, and its pathogenic G170R variant. *Biochimie* **92**, 1801–1811 https://doi.org/10.
     1016/j.biochi.2010.08.005

26   Burt, H.J., Pertinez, H., Sall, C., Collins, C., Hyland, R., Houston, J.B. et al. (2012) Progress curve mechanistic modeling approach for assessing
     time-dependent inhibition of CYP3A4. *Drug Metab. Dispos.* **40**, 1658–1667 https://doi.org/10.1124/dmd.112.046078

27   Gabadinho, J., Beteva, A., Guijarro, M., Rey-Bakaikoa, V., Spruce, D., Bowler, M.W. et al. (2010) MxCuBE: a synchrotron beamline control environment
     customized for macromolecular crystallography experiments. *J. Synchrotron. Radiat.* **17**, 700–707 https://doi.org/10.1107/S0909049510020005

28   Kabsch, W. (2010) Integration, scaling, space-group assignment and post-refinement. *Acta Crystallogr. D Biol. Crystallogr.* **66**(Pt 2), 133–144
     https://doi.org/10.1107/S0907444909047374

29   Evans, P.R. and Murshudov, G.N. (2013) How good are my data and what is the resolution? *Acta Crystallogr. D Biol. Crystallogr.* **69**(Pt 7), 1204–1214
     https://doi.org/10.1107/S0907444913000061

30   Collaborative Computational Project Nimber 4. (1994) The CCP4 suite: programs for protein crystallography. *Acta Crystallogr. D Biol. Crystallogr.* **50**(Pt
     5), 760–763 https://doi.org/10.1107/S0907444994003112

31   Vagin, A. and Teplyakov, A. (2010) Molecular replacement with MOLREP. *Acta Crystallogr. D Biol. Crystallogr.* **66**, 22–25 https://doi.org/10.1107/
     S0907444909042589

32   Emsley, P. and Cowtan, K. (2004) Coot: model-building tools for molecular graphics. *Acta Crystallogr. D Biol. Crystallogr.* **60**(Pt 12 Pt 1), 2126–2132
     https://doi.org/10.1107/S0907444904019158

33   Murshudov, G.N., Skubak, P., Lebedev, A.A., Pannu, N.S., Steiner, R.A., Nicholls, R.A. et al. (2011) REFMAC5 for the refinement of macromolecular
     crystal structures. *Acta Crystallogr. D Biol. Crystallogr.* **67**(Pt 4), 355–367 https://doi.org/10.1107/S0907444911001314

34   Davis, I.W., Leaver-Fay, A., Chen, V.B., Block, J.N., Kapral, G.J., Wang, X. et al. (2007) Molprobity: all-atom contacts and structure validation for
     proteins and nucleic acids. *Nucleic Acids Res.* **35**, W375–W383 https://doi.org/10.1093/nar/gkm216

35   Cellini, B., Montioli, R., Paiardini, A., Lorenzetto, A. and Voltattorni, C.B. (2009) Molecular insight into the synergism between the minor allele of human
     liver peroxisomal alanine:glyoxylate aminotransferase and the F152I mutation. *J. Biol. Chem.* **284**, 8349–8358 https://doi.org/10.1074/jbc.
     M808965200

36 Conter, C., Oppici, E., Dindo, M., Rossi, L., Magnani, M. and Cellini, B. (2019) Biochemical properties and oxalate-degrading activity of oxalate decarboxylase from *Bacillus subtilis* at neutral pH. *IUBMB Life.* **71**, 917–927 https://doi.org/10.1002/iub.2027

37 Purdue, P.E., Allsop, J., Isaya, G., Rosenberg, L.E. and Danpure, C.J. (1991) Mistargeting of peroxisomal L-alanine:glyoxylate aminotransferase to mitochondria in primary hyperoxaluria patients depends upon activation of a cryptic mitochondrial targeting sequence by a point mutation. *Proc. Natl Acad. Sci. U.S.A.* **88**, 10900–10904 https://doi.org/10.1073/pnas.88.23.10900

38 Beeler, T. and Churchich, J.E. (1976) Reactivity of the phosphopyridoxal groups of cystathionase. *J. Biol. Chem.* **251**, 5267–5271 PMID:8458

39 Cortijo, M., Jimenez, J.S. and Llor, J. (1978) Criteria to recognize the structure and micropolarity of pyridoxal 5′-phosphate-binding sites in proteins. *Biochemical J.* **171**, 497–500 https://doi.org/10.1042/bj1710497

40 Deller, M.C. and Rupp, B. (2015) Models of protein–ligand crystal structures: trust, but verify. *J. Comput. Aided Mol. Des.* **29**, 817–836 https://doi.org/10.1007/s10822-015-9833-8

41 Ikushiro, H., Hayashi, H. and Kagamiyama, H. (2004) Reactions of serine palmitoyltransferase with serine and molecular mechanisms of the actions of serine derivatives as inhibitors. *Biochemistry* **43**, 1082–1092 https://doi.org/10.1021/bi035706v

42 Brenton, A.G. and Godfrey, A.R. (2010) Accurate mass measurement: terminology and treatment of data. *J. Am. Soc. Mass Spectrom.* **21**, 1821–1835 https://doi.org/10.1016/j.jasms.2010.06.006

43 Behnam, J.T., Williams, E.L., Brink, S., Rumsby, G. and Danpure, C.J. (2006) Reconstruction of human hepatocyte glyoxylate metabolic pathways in stably transformed Chinese-hamster ovary cells. *Biochem. J.* **394**(Pt 2), 409–416 https://doi.org/10.1042/BJ20051397

44 Oppici, E., Roncador, A., Montioli, R., Bianconi, S. and Cellini, B. (2013) Gly161 mutations associated with primary hyperoxaluria type I induce the cytosolic aggregation and the intracellular degradation of the apo-form of alanine:glyoxylate aminotransferase. *Biochim. Biophys. Acta* **1832**, 2277–2288 https://doi.org/10.1016/j.bbadis.2013.09.002

45 Asano, N., Ishii, S., Kizu, H., Ikeda, K., Yasuda, K., Kato, A. et al. (2000) In vitro inhibition and intracellular enhancement of lysosomal alpha-galactosidase A activity in Fabry lymphoblasts by 1-deoxygalactonojirimycin and its derivatives. *Eur. J. Biochem.* **267**, 4179–4186 https://doi.org/10.1046/j.1432-1327.2000.01457.x

46 Khanna, R., Soska, R., Lun, Y., Feng, J., Frascella, M., Young, B. et al. (2010) The pharmacological chaperone 1-deoxygalactonojirimycin reduces tissue globotriaosylceramide levels in a mouse model of Fabry disease. *Mol. Ther.* **18**, 23–33 https://doi.org/10.1038/mt.2009.220

47 Mena-Barragan, T., Garcia-Moreno, M.I., Sevsek, A., Okazaki, T., Nanba, E., Higaki, K. et al. (2018) Probing the inhibitor versus chaperone properties of sp(2)-iminosugars towards human β-glucocerebrosidase: a picomolar chaperone for gaucher disease. *Molecules* **23**, E927 https://doi.org/10.3390/molecules23040927

48 Trapero, A. and Llebaria, A. (2013) Glucocerebrosidase inhibitors for the treatment of Gaucher disease. *Future Med. Chem.* **5**, 573–590 https://doi.org/10.4155/fmc.13.14

49 Malashkevich, V.N., Strop, P., Keller, J.W., Jansonius, J.N. and Toney, M.D. (1999) Crystal structures of dialkylglycine decarboxylase inhibitor complexes. *J. Mol. Biol.* **294**, 193–200 https://doi.org/10.1006/jmbi.1999.3254

50 Schade, S. and Paulus, W. (2016) D-cycloserine in neuropsychiatric diseases: a systematic review. *Int. J. Neuropsychopharmacol.* **19**, pyv102 https://doi.org/10.1093/ijnp/pyv102